ACS Sustainable Chem. Eng. 4 (2016) 2487-2494

DOI: 10.1021/acssuschemeng.5b01444

Mn containing N-doped monolithic carbon aerogels with enhanced macroporosity as electrodes for capacitive deionization

Carlos Macías[1], *Gloria Rasines*[1], *Pedro Lavela*[2]*, *María C. Zafra*[2], *José L. Tirado*[2], *Conchi O. Ania*[3].

[1] I+D Department, Nanoquimia S.L., PCT Rabanales 21, Ed. Aldebarán M.4.7. 14014 Córdoba, Spain.

[2] Laboratorio de Química Inorgánica, Universidad de Córdoba, Marie Curie, Campus de Rabanales, 14071 Córdoba, Spain.

[3] Adsorption and Environmental Remediation on Porous Solids (ADPOR), Instituto Nacional del Carbón, INCAR-CSIC, Apdo. 73, 33080 Oviedo, Spain.

KEYWORDS Resorcinol; Desalination; Nitrogen doping; Manganese;Carbon black; Diatomite.

ABSTRACT

We propose the use of siliceous diatomite as an anti-shrinkage additive for the synthesis monolithic carbon aerogel electrodes with enhanced electrochemical response for capacitive deionization of NaCl solutions. Hybrid N- and Mn-doped carbon aerogels with improved electrical conductivity and wettability in the aqueous electrolyte are prepared by introducing modifications in the synthesis (carbon black and/or diatomite loading before the polymerization sol-gel polycondensation of the monomers, followed by manganese infiltration). The textural and morphological characterization of the materials reveals that the presence of the additives does not impede the cross-linking of the monomers to form branched clusters and colloidal aggregates leading to a highly porous structure. Furthermore, the aerogels materials display an open macroporous network inherited by the diatomite, even after its lixiviation. As a result, the monolithic carbon aerogel electrodes present good electrochemical performance in terms of low polarization resistance, high capacitance and fast electroadsorption.

Introduction

Highly porous carbon aerogels are nowadays a matter of subject because of their use as electrodes in adsorption/energy applications. They are outstanding materials because they combine beneficial adsorption properties and structural strength with suitable chemical stability and electronic conductivity.[1-5]Carbon aerogels are a cost effective solution in applications aiming ion removal, as capacitive deionization. Their high surface area and pore volume exert a crucial role as capacitive electrodes that physically adsorb ions from the electrolytic solution. This reversible process present remarkable advantages for brackish water desalination.[6-10]New strategies point out to optimal morphologies,[11, 12] innovative preparative routes,[13, 14]and hybrid multifunctional materials for providing both an open structure and suitable electrochemical behavior.[15-17]

It could be expected that the use of anti-shrinkage additives, that limit the contraction of the aerogel upon carbonization and create a macroporous structure, may contribute favorably to improve their electrosorption behavior.[18] Diatomaceous earth is a non-toxic and low cost material typically used as reinforcing and anti-shrinkage additive preserving macroporosity.[19, 20]We have recently reported mechanically compliant and highly porous aerogels with enhanced electrical conductivity prepared in the presence of diatomaceous earth and carbon black as additives. These materials overcome the limitations of mechanical stiffness upon densification by carbonization, while maintaining outstanding porous features and improved electrical conductivity, both desirable characteristics for the implementation of the monolithic aerogels in electrochemical applications.[21] On the other hand, the reliability of N-doped carbons as electrodes for capacitive deionization has been evidenced.[22, 23]. Also, the presence of a

macropore structure in the monolithic configuration was revealed as a crucial factor for a fast electrosorption of ions during the salt deionization.[23]

Unfortunately, the sole use of diatomite templating treatment in carbon aerogels has demonstrated to be insufficient to increase capacitance in the first attempts, even if the kinetic response is clearly improved due to the macroporous structure. For this reason, we propose that the combination of capacitive effect from carbon aerogels and pseudo-faradaic reactions in transition metal compounds may contribute favorably to enhance the electropsortion capacities of new electrodes for capacitive deionization.[24]

Taking all this into account, the aim of this work was the preparation of hybrid manganese-N doped carbon aerogels with enhanced macroporosity for their application as electrodes for the electrosorption of NaCl from aqueous solution. The use of a pre-polymerization route allows an efficient polymerization of the precursors yielding highly mesoporous aerogels with high N-contents, while diatomite was also used as anti-shrinkage additive.

Experimental

Hydrogels were synthesized by the polycondensation of Melamine (M), Resorcinol (R) and Formaldehyde (F) using sodium carbonate as catalyst (C) and deionized water (W) as solvent. Carbon black (CB, Superior Graphite Co.) and diatomite (D, Nanolit K-6) were used as conductive and anti-shrinkage additives, respectively. The molar ratios of reactants were as follows: R:M:F of 2:1:7, (M+R)/C of 135 and (M+R)/W of 0.053. The final pH of the precursors was adjusted to 7.4 by adding sodium carbonate. The samples were synthesized according to a

prepolymerization procedure described elsewhere.[23] Before gelification, diatomite (50%w/v) and/or carbon black (0.75% w/v) were added to the mixture and magnetically stirred to ensure a homogeneous dispersion. Hydrogels were then kept in an oven at 40 ºC for 24 h and then at 70 ºC for 120 h to allow gelation and aging. After a controlled water–acetone exchange, the hydrogels were supercritically dried with CO_2 and carbonized (ca. 2 ºC/min) at 480 ºC under nitrogen atmosphere. Since the diatomite is electrically non-conductive and may hinder the access of ions to the mesoporous system, it was etched-off using HF and leaving a silica free carbon monolith. Then, selected samples were doped with manganese by immersing the gel in a $Mn(NO_3)_2$ solution followed by heating up to 750 ºC for 120 min in CO_2 atmosphere. Samples will be named as MRF-X-Y-Z, where X,Y and Z respectively indicates the presence of manganese (Mn), diatomite (D) and carbon black (B), respectively.

Wettability was determined by measuring the contact angle between the electrolyte and the electrode material in both powdered and monolithic forms. It is calculated from the tangent angle of the liquid drop with a solid surface at the base. High resolution nitrogen adsorption/desorption isotherms at -196 ºC were measured for the samples in a volumetric analyzer (ASAP 2010, Micromeritics) equipped with high-vacuum system, and three pressure transducers. The samples were degassed under vacuum at 120 ºC overnight prior to the adsorption measurements. Ultrahigh purity nitrogen (i.e., 99.9992%) was supplied by Air Products. Each isotherm measurement was performed in duplicate to guarantee the reproducibility and accuracy of the measurements (error was below 0.1%). The specific surface area, S_{BET} and total pore volume, V_T were calculated from the isotherms according to the Brunauer–Emmett–Teller theory, while the full micro-meso pore size distribution was calculated using the 2D-NLDFT-HS model [25] assuming surface heterogeneity of carbon pores.[26] Mercury porosimetry was performed in a

Micromeritics Autopore IV apparatus working in the pressure range 1–2000 bars was used. X-Ray diffraction (XRD) patterns were recorded on a Siemens D5000 diffractometer equipped with a graphite monochromator and Cu Kα radiation. The samples were scanned between 10º and 90º (2θ) at a 0.02◦/12 s scan rate. X-ray Photoelectron spectrometry was carried out in a XPS, SPECS Phobios 150MCD equipment provided with a X-ray monochromatic Al K (1486.61 eV) power source of 300 W (anode voltage of 12 kV). The base pressure in the ultra high vacuum chamber was 4×10^{-9} mbar. Binding energy values were referenced to the C 1s peak of the adventitious carbon at 284.6 eV before the spectra processing.[27] The accurate determination of the binding energy and relative contribution of the signals was achieved by decomposing the overall profile in Gauss–Lorentz curves with a CasaXPS software package. Elemental analysis was performed in Eurovector EA 3000 equipment. Scanning electron microscopy (SEM) was performed in a Quanta FEG 650 equipment furnished with a S/TEM detector. Transmission electron microscopy (TEM) images were recorded in a JEOL JEM 2010 microscope.

The electrochemical characterization of the carbon aerogel electrodes was performed in three-electrode Swagelok™ type cells. The working electrode consisted of a homogeneous mixture composed by the carbon active material (70 wt.%), carbon black (Superior graphite, 20 wt.%) and PVDF binder (10 wt.%) dispersed in N-methyl pyrrolidone. The slurry was cast on 13 mm titanium disks and dried at 70ºC overnight. A Hg/Hg_2SO_4 (SME) and a platinum wire were respectively used as reference and counter electrodes. The electrolyte was a 0.1 M NaCl solution in deionized water. Cyclic voltammograms and galvanostatic cycles were performed between -0.5 and +0.5 V versus the reference electrode using a Biologic VMP multichannel potentiostat to control the process. Electrochemical impedance spectroscopy (EIS) was employed to determine the internal resistance at the electrode interphases. During the experiment, the cell is perturbed

by an AC voltage signal of 5 mV vs equilibrium potential over the frequency range 25 kHz to 10 mHz.

A symmetrical batch-type cell was assembled to perform the capacitive deionization experiments. The electrodes were two monolithic aerogel electrodes weighing ca. 0.15 g and ca. 0.3 cm^3. Their surfaces were polished to ensure a good contact with the current collector. Then, the pieces were washed in deionized water for 30 minutes. The electrodes were sandwiched between titanium current collectors and separate by two Whatman glass GF/A fiber sheets. Then, they were immersed into 15 mL of a 0.025 Mor 0.1 M NaCl solution magnetically stirred to favor mass transfer from the bulk solution to the electrode. The cell was charged by applying a potentiostatic pulse (0.9, 1.2 or 1.5 V for 120 or 150 min) using an Arbin BT2000 multichannel potentiostat. Afterwards, the electrodes were discharged at 0 V for the same period of time. A conductivity-meter Crison EC meter BASIC 30 was used to monitor the changes of the ionic conductivity.

Results and discussion

Figure 1 shows images of the monolithic carbon aerogel materials prepared in the presence and absence of the various additives used. A simple visual inspection of the pieces evidences the significant shrinkage (ca. 25-35 % reduction of diameter) of the specimen prepared in the absence of the diatomaceous anti-shrinkage additive, induced by the thermal treatment at 750ºC. On the contrary, when the siliceous additive was incorporated in the synthesis, the pieces preserved their size and shape after the carbonization and further washing with HF (ca. 5% reduction in the diameter of the specimens). The anti-shrinkage effect of the diatomite is not

dependent on the formulation of the aerogel or the presence of the carbon black conductive additive.[23] In addition, the aerogels ranged from translucent (pristine MRF) to opaque when either B or D additives were used, due to the relatively large amounts of additives added. The wettability of carbon aerogels can be visualized in Fig. S1. These images reveal the highly hydrophilic character provided by the diatomite treatment which undoubtedly will ensure a proper impregnation and hence a suitable electrode-electrolyte intephase. Otherwise, the contact angles for MRF and MRF-Mn were respectively 42^{o} and 71^{o}, indicating that the sole deposition of Mn containing particle negatively affects to its wettability.

The incorporation of the diatomaceous additive created macropores, as seen in the SEM images (Figure 1). Sample MRF is characterized by a relatively smooth surface in which the carbon particles appear densely packed. At converse, MRF-Mn-D monolith displayed a rough surface with large holes, likely created during the etching off the diatomite after the acid washing. It was corroborated by the bulk density values of the monoliths (Table 1). Those samples prepared in the absence of additives -i.e., MRF and MRF-Mn-, featured a density value of 0.40 cm^3 g^{-1}, similar to those reported in the literature.[28]Upon the incorporation of diatomite, there is a notorious decrease in the bulk density to values close to 0.15 cm^3 g^{-1}, due to the large voids inherited from the additive. The TEM images show the dispersion of the metallic aggregates in the aerogel matrix (Figure S2, Supporting Information); MRF-Mn aerogel features typical aggregates with a relatively compacted morphology which yield the mesoporous network. In the case of MRF-Mn-D-CB, the large voids are also observed, along to dark spots belonging to the manganese and/or carbon black particles.

Figure 2 shows the N_2 adsorption isotherms of the prepared materials; the main textural parameters are also compiled in Table 1. All the materials displayed high porous features,

confirming that the incorporation of the additive (either B or D) does not hinder the polycondensation of the reactants.[29-31] All the materials displayed type IV isotherms according to IUPAC classification[32] with relatively high adsorbed volume at relative pressures below 0.2 (corresponding to micropore range) and well-defined hysteresis loop in the desorption branches at relative pressures higher than 0.7, evidencing their mesoporous character. The large pore volumes and hysteresis loops in the gas adsorption data suggest that the polycondensation of the monomers is slowed down in the presence of the additives (either B or D). This would lead to a lower degree of cross-linking of the structure, generating weakly branched clusters that tend to form larger colloidal aggregates in progressively larger pores (mesopore coarsening).[29]

The incorporation of diatomite provoked a slight fall in the pore volumes, whereas the microporosity followed a slightly increasing trend (Table 1). Consequently, the aerogels prepared in the presence of the additives displayed higher surface area values than the pristine MRF gel, although all the samples are highly microporous. Otherwise, the addition of carbon black (sample MRF-Mn-D-CB) yielded an increase in the mesopore volume (compared to MRF-Mn-D), as commonly observed for similar composite aerogels.[30, 31].

The impact of the additives on the texture of the carbon aerogels can also be seen in the pore size distributions (Figure 2b). In agreement with the shape of the isotherms, there is an increase in the contribution to pore widths smaller than 1 nm. Concerning mesopores, carbon aerogels treated with diatomite feature a multimodal distribution with several peaks between 5 to 25 nm. Moreover, an analysis of the pore size distribution measured by mercury porosimetry reveals an additional contribution of macropores (500 nm) in samples MRF-Mn-D and MRF-Mn-DB which is not present in the material synthesized in the absence of the diatomite (Fig. 2c). The sample incorporating the carbon black also displayed a contribution of large voids above 10 micron.

This result clearly shows the capability of the siliceous additive to modify the porous network of the carbon matrix creating large voids in the meso-/macropore range.

The chemical composition of aerogels was determined by elemental analysis and XPS (Table S1, Supporting Information). As expected, the incorporation of manganese caused a decrease in the carbon and nitrogen contents. Otherwise, XPS data revealed an increase in the overall content of oxygen in the Mn-containing aerogels, suggesting the formation of manganese oxides. No crystalline manganese phases were detected by X-ray diffraction (Fig. S3 Supporting Information), which we attribute to the low manganese content of the samples (Table S1, Supporting Information). On the other hand, the amount of nitrogen from the chemical analysis is slightly higher than that obtained from the XPS spectra. This evidences that the N-containing groups are not located at the surface of the aerogel, but also efficiently incorporated in the bulk material; hence the concentration of the doping element is lower near the surface.[33, 34] Furthermore, the amount of nitrogen groups is similar to all the samples, which confirms the efficient polymerization of the reactants in the presence of the additives.

To evaluate the influence of the additives on the nature of the different N- and O-groups, the surface chemistry of the aerogels was investigated by XPS. Five different gaussian-lorentzian components were deconvoluted from the C1s core level spectra(Figure S4,Supporting Information). The main signals were assigned to graphitic carbon in a sp^2 configuration, 284.6±0.1 eV), Csp^2–N/C–OH (285.8±0.1 eV), Csp^3–N/C=O (287.1±0.1 eV), and carboxyl (289.2±0.2 eV) groups. A shake-up satellite peak due to π-π* transitions in aromatic rings appears ca. 291.1±0.1 eV as a low intense and highly broadened band.[35] The relative contributions of the different peaks are compiled in Table 2. As seen, the contribution of the graphitic carbon prevails over other surface functionalities, regardless the carbon aerogel. The

presence of the diatomite in MRF-Mn-D led to a slightly higher contribution of Csp^2–N/C–OH, while Csp^3−N/C=O significantly decreased. These tendencies were confirmed by the relative contributions of the signals ascribable to C=O in ketone/carbonyl (531.2±0.2 eV) and O-C in lactone, phenol, ether, epoxy (533.0±0.2 eV) in the O1s core level spectra (Figure S5, Supporting Information and Table 2). Three additional signals attributed to C=O in carboxylic acids (534.4±0.1 eV), adsorbed and/or occluded CO/CO_2 (536.2±0.2 eV), and trapped CO and CO_2 molecules (536.2 eV) coming from the thermal decomposition of traces of carbonate used as catalyst were detected in the deconvolution of the O1s core level spectra.[36-38]

The spectra at the N1s core level were decomposed into four overlapped bands assigned to N6 pyridinic (398.3±0.2 eV), N5 pyrrolic/pyridone (400.2±0.2 eV), N-Q quaternary (401.5±0.2 eV) and (N-X) pyridine N-oxide (403.5±0.1 eV).[39-41] N-6 and N-5 groups were the dominant species, while all the samples presented somewhat similar relative distributions (Figure S6, Supporting Information andTable 2). This indicates that the nitrogen atoms incorporated in the polymerization reaction, are not affected by the incorporation of the additives. On the other hand, the chemical state of manganese was also explored from XPS spectroscopy. Figure3 shows the spectra of the $Mn2p_{3/2}$ core level; the profiles were decomposed in three components at ca. 640.8 ±0.1, 642.4±0.1 and 644.9±0.1 eV, which were assigned to Mn(III), Mn(IV) and shake-up satellites, respectively.[42, 43]

It could be envisaged that the macroporous network and the improved electrical conductivity of thesecomposites -due to the incorporation of the carbon black additive and the occurrence of electron donating N-groups,[44-46]may lead to an enhancement of the kinetic response at the electrode–electrolyte interface.[47]To evaluate the polarization resistance of the electrodes, impedance spectroscopy was performed. The Nyquist plots are displayed in Figure 4; the profiles

appeared significantly distorted due to the complex porous structure of the aerogels (Table 1), but all of them displayed a semicircle at high and intermediate frequencies prolonged by a straight line. The polarization resistance values (R_{pol}) were calculated by fitting the experimental data to the equivalent circuit depicted in Figure4b -consisting of the electrolyte solution resistance (R_{el}), the polarization resistance (R_{pol}), the Warburg impedance (W), a constant phase element (CPE) and a capacitor (C). The resistance of the electrolyte solution is so low that its contribution to the overall resistance can be neglected. Thus the polarization resistance is mainly responsible for the internal electrode resistance, and varied upon the trend: MRF-Mn-D-CB (0.45 Ω×g), MRF-Mn-D (0.57 Ω×g), MRF (0.79 Ω×g) and MRF-Mn (1.02 Ω×g). These results clearly reveal the beneficial effect of the incorporation of the diatomite in the synthesis of the carbon aerogels, providing lower polarization resistance values than the materials prepared in the absence of the siliceous additive. This can be attributed to the macropore structure, inherited by the anti-shrinkage additive and the effect of the carbon black. Contrarily, the highest polarization resistance of MRF-Mn reveals that the single combination of the Mn phase with MRF is not an optimal solution. Likely, the less hydrophilic character of this aerogel hinders the formation of an optimal electrode electrolyte interphase that would eventually counterbalance the favorable accessibility provided by the high specific surface and pore volume.

The capacitive behavior was evaluated from the cyclic voltammograms recorded in 3-electrode cells (Figure5). The profiles for MRF and MRF-Mn show the typical box-like shape ascribable to a capacitive behavior resulting from the electrostatic interactions between the charged electrode and opposite ions coming from the electrolyte. The positive slopes observed at extreme potential values are due to restricted ion diffusion into the micropores leading to an electrode resistivity and slight decomposition of the electrolyte.[48] In the case of the aerogels prepared in

the presence of the diatomite (samples MRF-Mn-D-CB and MRF-Mn-D), slight deviations from the rectangular shape are observed; the broad hump in the anodic sweep can be attributed to the presence of manganese and/or O- and N-groups promoting pseudo-faradaic reactions.[21, 23]In addition, Porada et al. have also indicated that chemical reactions as chloride oxidation at the anode, oxygen reduction at the cathode, and carbon oxidation are faradic contributions.[8]Thisbehavior is not so clearly seen in MRF-Mn, which might be attributed to the lower density of N- and O- groups of this material (Table S1), and/or the lower accessibility of the electrolyte to the metallic particles.

The electrochemical capacitance of MRF was 90±3 F g^{-1}, whilethat of MRF-Mn was of 86±3 F g^{-1}.It is slightly lower than that for MRF, or even indistinguishable whether the error margins are considered. Thus, the mere presence of the manganese phase was not determining for a capacitance improvement despite of the larger textural features of the former sample (Table 1). Likely, the poor wettability is a crucial factorlimiting the electrosorption of MRF-Mn.The highest capacitance values recorded for the MRF-Mn-D and MRF-Mn-D-CB aerogels -values of 104±2 and 113±1 F g^{-1}, respectively- are a direct consequence of the enhanced macroporosity and improved wettability of the diatomite treated aerogels. Thus, a synergic effect is exerted allowing the development of both electric double layer and pseudo-capacitive, due to ion adsorption through charge-transfer reactions, effects that contribute to the achievements of high capacitance values. This behavior was confirmed by galvanostatic cycling at different current densities (Fig. S7). Thus, capacitance values of 91 and 121 Fg^{-1} were respectively recorded for MRF and MRF-Mn-D-CB at 0.1 Ag^{-1}, which agrees well with tendency showed by the cyclic voltammograms.

Monoliths of the aerogels were assembled in symmetric cells to determine their electrosorption capacity in 0.025 M (ca. 1.5 g/L) NaCl solutions. The electroadsorption curves at different voltages and subsequent discharges at 0 V are plotted in Figure6. Interestingly, there does not seem to be a direct relationship between the capacitance values determined in the above-described 3-electrode cell configuration and the electrosorption capacity recorded in the 2-cell system after 120 minutes. The obtained values were quite similar for all the aerogels. For instance, a capacity of 6.7 mg of NaCl /g was observed for MRF, very close to the value measured for MRF-Mn-D-CB (ca. 6.1 mg/g), the best performing material evaluated by cyclic voltammetry (Figure 5).

This apparent disagreement can be interpreted by considering the different kinetic response of electrodes in a monolithic form, compared to powder ones.[30]The charge curve was steeper for MRF-Mn-Dand MRF-Mn-D-CB, with maximum capacities being reached after 60 minutes of charge. In the case of the pristine electrodes (no additives), the profiles displayed a fast response after 60 min followed by a second process (seen as a plateau in the charge curves) up to 120 min when the material is slowly charged. The highest adsorption capacities recorded at 0.9 V corresponded to the diatomite treated MRF-Mn-D-CB, regardless the time of charge. On increasing the applied voltage to 1.2 and 1.5 V, the improved kinetic behavior of the treatment with diatomite is more clearly evidenced because of their higher adsorption capacities for short times. For instance, the monoliths of MRF-Mn-D-CB adsorbed 4 mg/g after 20 minutes at 1.5 V, while only 2.2 mg/g were absorbed by the MRF aerogel (Figure S8).

To verify this assumption, further experiments were performed at a higher NaCl concentration (0.1 M) and longer adsorption times (150 minutes) for 1.5 V (Fig. 7 and S9). In these more demanding conditions, MRF-Mn-D-CB (7.9 mg/g) evidenced to perform better than MRF

aerogel. These results reveal the synergic effect of manganese containing particles, carbon black along with the diatomite treating to reach a carbon aerogel with optimized properties for capacitive deionization.

Conclusions

The use of a siliceous diatomite as anti-shrinkage additive has allowed the synthesis of carbon monolithic carbon aerogels with a well-developed micro and mesopore structure and enhanced macroporosity. The incorporation of nitrogen functionalities and carbon black as conductive additive enable to increase the electrical conductivity and wettability of the materials. The resulting carbon matrix have demonstrated to be a favorable support for manganese containing particles, which pseudofaradic effect contributes positively to the overall capacitance. These characteristics are responsible for the good electrochemical performance of the electrodes for the removal of ionic species in terms of fast kinetics and low resistance.

The morphological analysis showed the efficient anti-shrinkage effect and the sponge-like texture of the carbon aerogels after the diatomite removal. The nitrogen isotherms also revealed that the polycondensation of the reactants is not impeded by the presence of the additives (both diatomite and carbon black), leading to a multimodal distribution of pore sizes with mesopores. Concerning the deionization capacity measured in symmetric cells using monolithic electrodes, the aerogels synthesized in the presence of the diatomite showed a more advantageous response at low voltages and/or short charge time. These results demonstrate that the use of diatomite as anti-shrinkage additive can be a helpful solution to prepare highly porous carbon electrodes with optimized morphological properties for capacitive deionization.

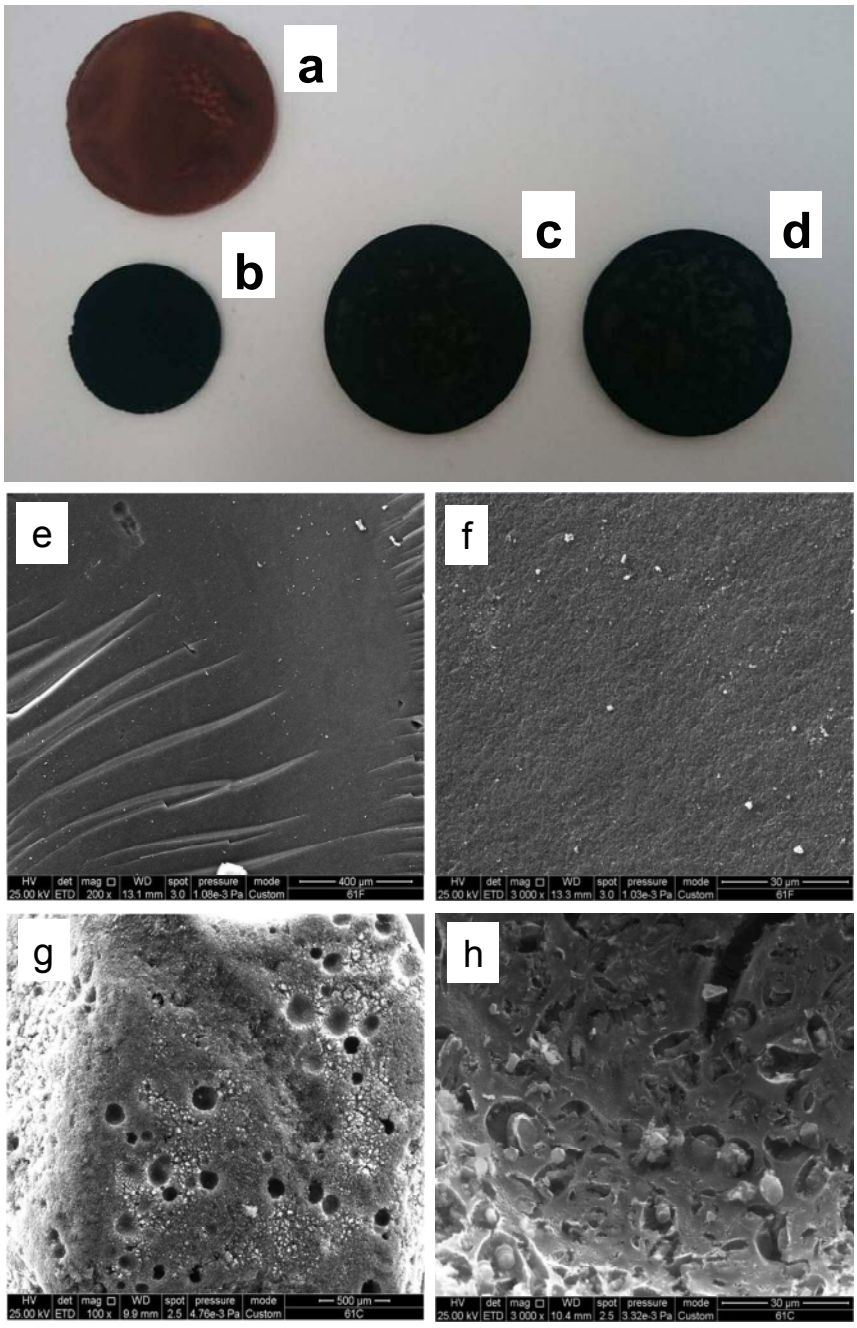

Figure 1. Images of the MRF hydrogel before (a) and after (b) carbonization (a), and the carbonized samples prepared in the presence of additives: c) MRF-Mn-D; d) MRF-Mn-D-CB. SEM images of (e, f) MRF/Act and (g, h) MRF-D/Act.

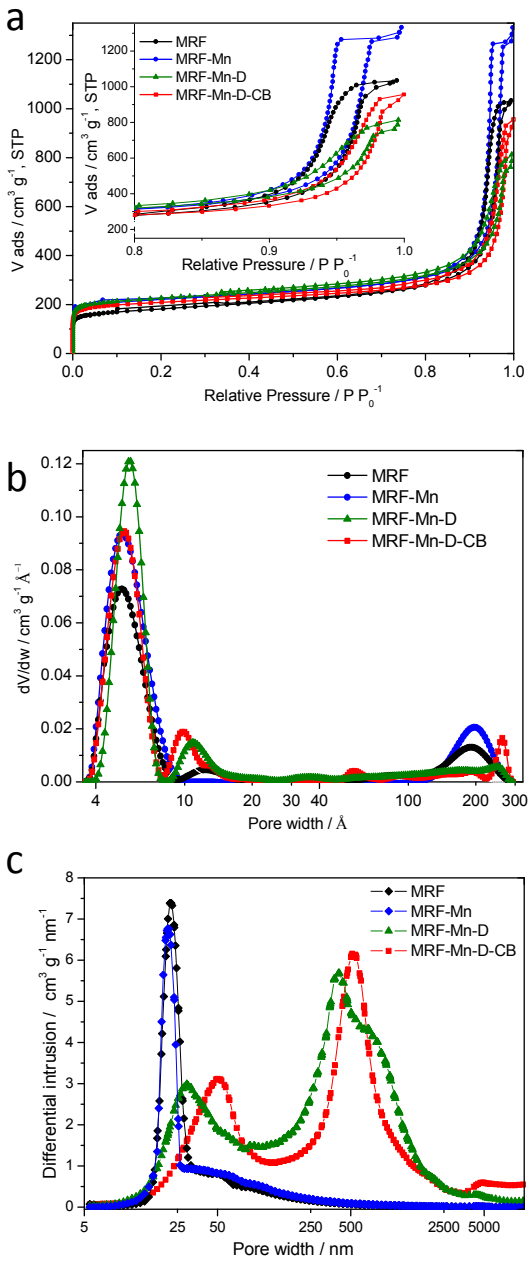

Figure 2. a) N_2 adsorption isotherms at -196 ºC of the N-doped carbon aerogels. Inset: Magnification of the high relative pressure region to discern the hysteresis loops; b) Pore size distributions obtained by using the 2D-NLDFT-HS method; c) Pore size distribution in the meso-

/macropore range for samples MRF and MRF-Mn-D-CB, calculated from mercury porosimetry.

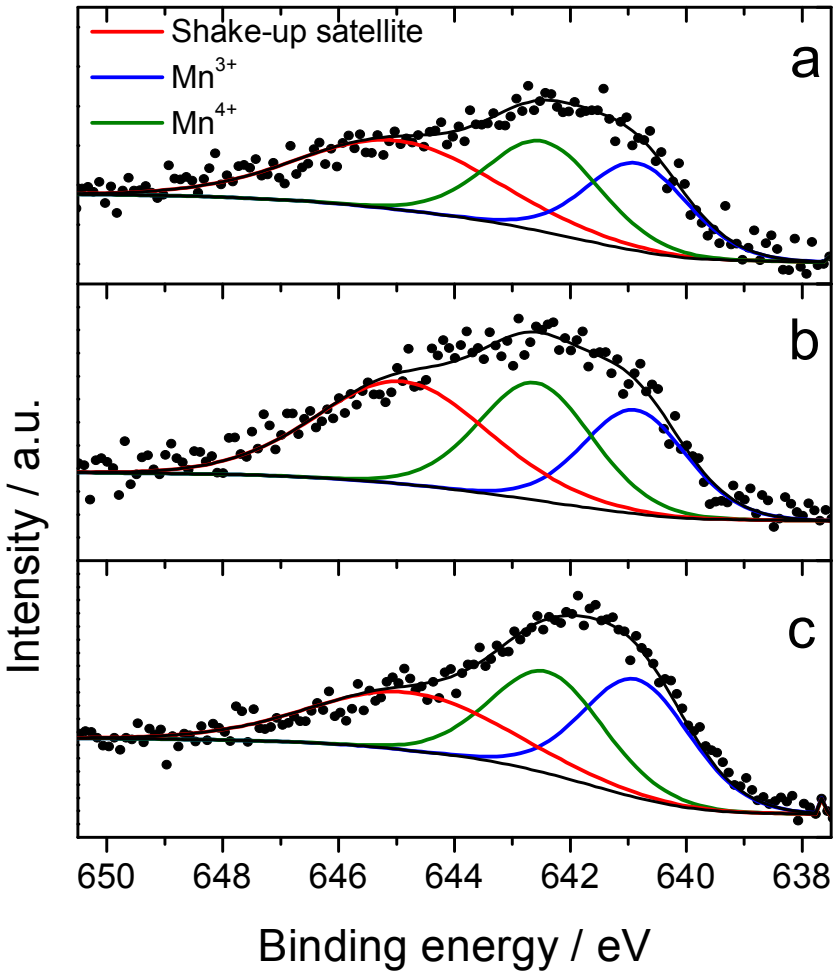

Figure 3. X-ray photoelectron spectra at the Mn $2p_{3/2}$ core level of a) MRF-Mn; b) MRF-Mn-D; c) MRF-Mn-D-CB.

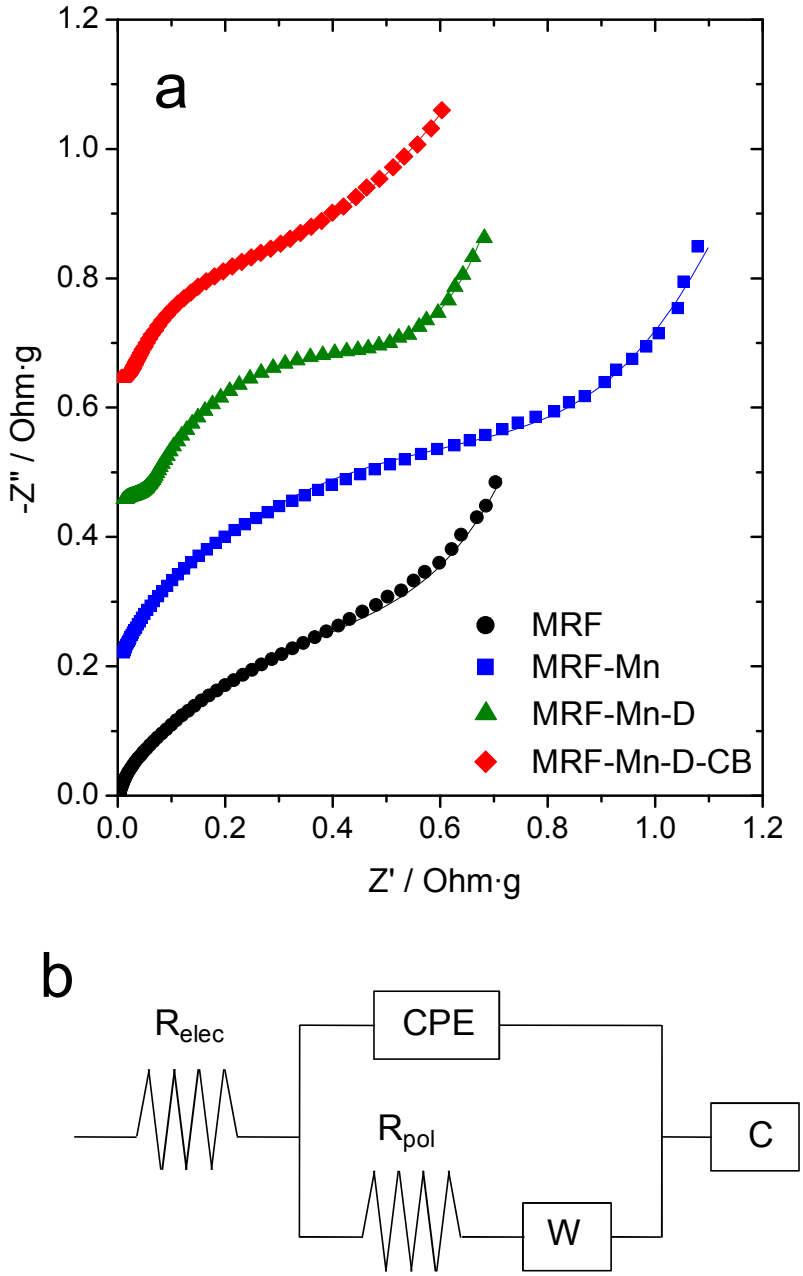

Figure 4. a) Nyquist plots derived from the impedance spectra recorded in the 0.1 M NaCl solution applying a modulated AC voltage signal of 5 mV vs the equilibrium potential; (b) Equivalent circuit used for the fitting of the spectra.

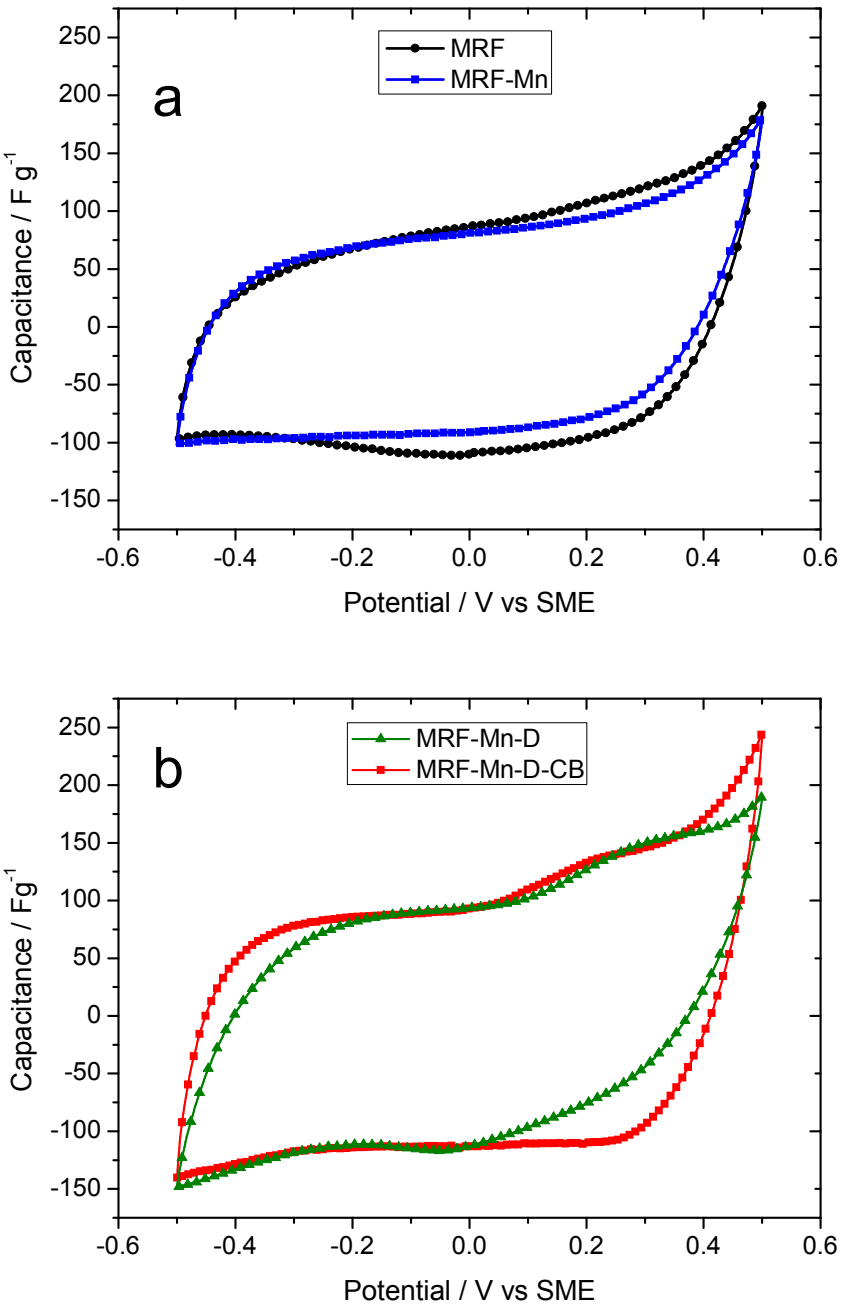

Figure 5. Cyclic voltammograms of MRF aerogel electrodes recorded in a 3-electrode cell configuration at 0.5 mV/s in 0.1 M NaCl solution.

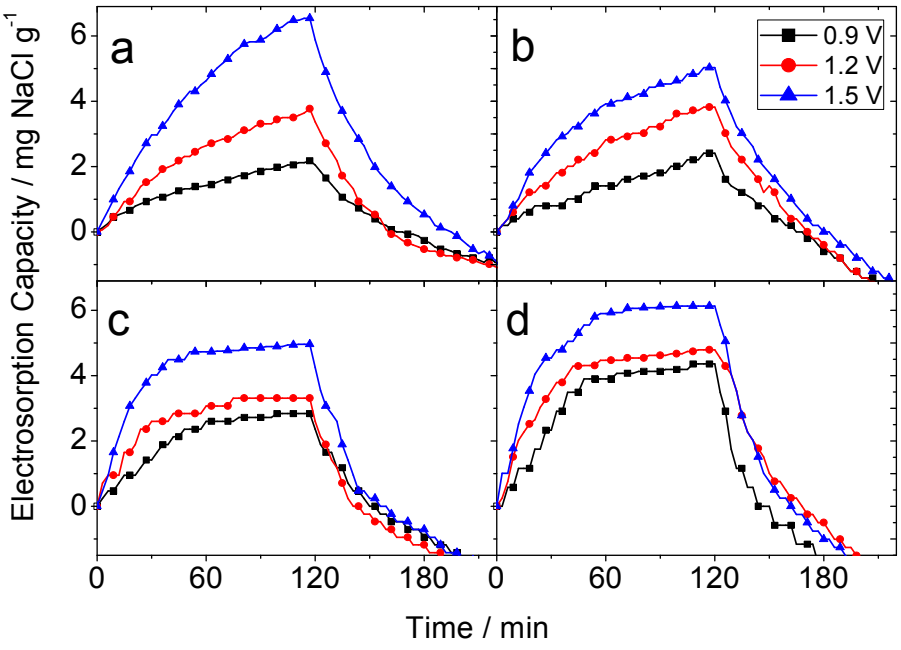

Figure 6. Capacitive deionization experiments performed at different potentials in 0.025 M NaCl (ca.1.5 g/L) solution for aerogels: a) MRF; b) MRF-Mn; c) MRF-Mn-D; f) MRF-Mn-D-CB.

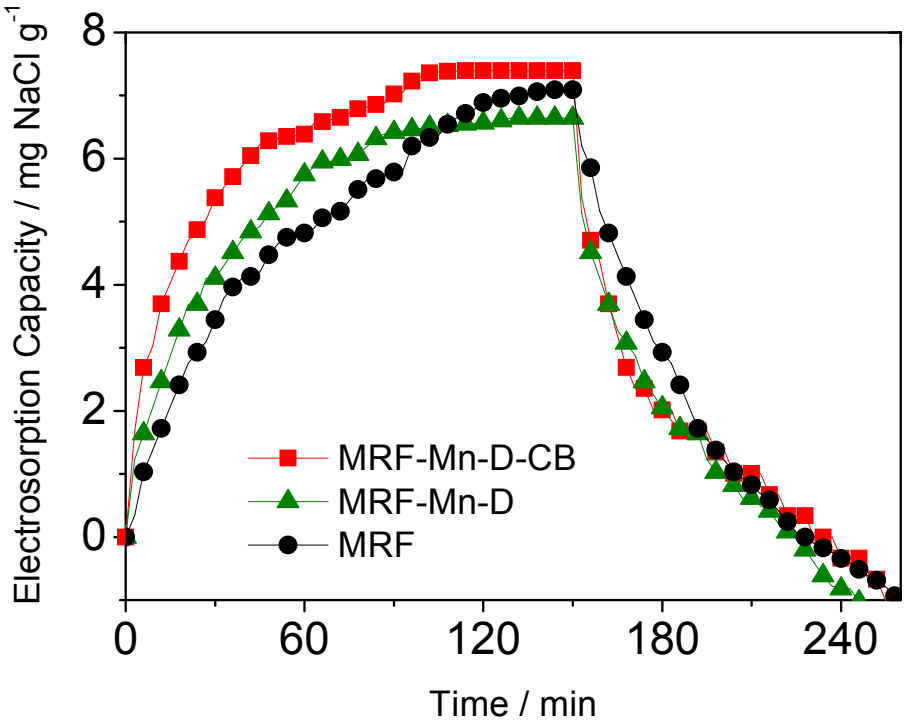

Figure 7. Capacitive deionization experiments performed at 1.5 V in 0.1 M NaCl (ca.6 g/L) solution for MRF,MRF-Mn-D and MRF-Mn-D-CBaerogels.

Table 1. Textural parameters of the composites containing N-doped carbon aerogels determined from the nitrogen isotherms at -196ºC, and monolith densities.

	S_{BET}	V_T [a]	V_{MIC} [b]	V_{MESO} [c]	Bulk density[d]
	$m^2\ g^{-1}$	$cm^3\ g^{-1}$	$cm^3\ g^{-1}$	$cm^3\ g^{-1}$	$g\ cm^{-3}$
MRF	679	1.58	0.21	1.35	0.40
MRF-Mn	844	1.96	0.25	1.76	0.40
MRF-Mn-D	862	1.17	0.29	0.86	0.15
MRF-Mn-D-CB	804	1.38	0.27	0.98	0.16

[a] total pore volume evaluated at $p/p_0 \sim 0.99$

[b, c] micro-, mesopore volume evaluated by the 2DNLDFT-HS method applied to the N_2 adsorption isotherms at 77 K

[d] Data calculated from the weight and geometrical dimensions of the monolith.

Table 2. XPS parameters calculated from the deconvolution of N 1s, O1s, C1s spectra of hybrid composite containing N-doped carbon aerogels (B.E.=binding energy)..

Envelope N1s				
Assignment	**N-6**	**N-5**	**N-Q**	**N-X**
MRF	35.2	40.7	15.7	8.5
MRF-Mn	32.6	44.7	16.2	6.4
MRF-Mn-D	35.4	43.3	14.3	6.9
MRF-Mn-D-CB	32.3	49.9	12.4	5.4
Envelope O1s				
Assignment	**C=O**	**C-O-**	**COO-**	**H_2O/ Occluded CO /CO_2**
MRF	21.0	51.4	23.8	3.8
MRF-Mn	12.2	59.7	25.6	2.4
MRF-Mn-D	16.3	59.4	21.5	2.9
MRF-Mn-D-CB	18.7	56.1	23.2	2.0
Envelope C1s					
Assignment	**C-C**	**Csp^2-N/ C−OH**	**Csp^3−N/ C=O**	**O-C=O**	**π-π***
MRF	60.5	15.3	12.1	9.0	3.0
MRF-Mn	58.5	17.8	13.3	9.0	1.3
MRF-Mn-D	60.5	21.2	8.8	9.3	0.3
MRF-Mn-D-CB	63.9	16.8	9.4	8.8	1.0

ASSOCIATED CONTENT

Wettability pictures, TEM images, XRD, XPS spectra for C1s, O1s and N1s core levels and chemical analysis data. This material is available free of charge via the Internet at http://pubs.acs.org."

AUTHOR INFORMATION

Corresponding Author

*(E-mail address: Pedro.Lavela@uco.es; Phone:34 957 218637.

ACKNOWLEDGMENT

The authors are indebted to the MINECO (Contract IPT-2011-1450-310000 (ADECAR) and FEDER cofunding, and CTM2014-56770-R) for the financial support. We also thank the fruitful collaboration of Isolux Ingeniería, S.A., Fundación Imdea Energía and Proingesa.University of Cordoba thanks to SCAI and IUIQFN for technical support and Junta de Andalucía (FQM-288) for financial support.

REFERENCES

(1) White, R. J.; Brun, N.; Budarin, V. L.; Clark, J. H.; Titirici, M. M. Always Look on the "Light" Side of Life: Sustainable Carbon Aerogels. *ChemSusChem***2014**, *7*, 670 – 689.

(2) Pekala, R. W.; Farmer, J. C.; Alviso, C. T.; Tran, T. D.; Mayer, S. T.; Miller, J. M.; Dunn, B. Carbon aerogels for electrochemical applications. *J. Non-Cryst. Solids***1998**, *225*, 74 – 80.

(3) Moreno-Castilla, C.; Maldonado-Hodar F. J. Carbon aerogels for catalysis applications: An overview. *Carbon***2005**, *43*, 455 – 465.

(4) Humplik, T.; Lee, J.; O'Hern, S. C.; Fellman, B. A.; Baig, M. A.; Hassan, S. F.; Atieh, M. A.; Rahman, F.; Laoui, T.; Karnik, R.; Wang, E. N. Nanostructured materials for water desalination. *Nanotechnology***2011**, *22*, 292001.

(5) S.A. Al-Muhtaseb, J.A. Ritter, Preparation and properties of resorcinol–formaldehyde organic and carbon gels, *Adv. Mater*. **2003**, *15*, 101-114.

(6) AlMarzooqi, F. A.; Al Ghaferi, A. A.; Saadat, I.; Hilal, N.; Application of Capacitive Deionisation in water desalination: A review. *Desalination***2014**, *342*, 3–15.

(7) Anderson, M. A.; Cudero A. L.; Palma, J. Capacitive deionization as an electrochemical means of saving energy and delivering clean water. Comparison to present desalination practices: Will it compete? *Electrochim. Acta***2010**, *55,* 3845–3856.

(8) Porada, S.; Zhao, R.; van der Wal, A.; Presser, V.; Biesheuvel, P. M. Review on the science and technology of water desalination by capacitive deionization. *Prog. Mater. Sci.***2013**, *58*, 1388–1442.

(9) Oren, Y. Capacitive deionization (CDI) for desalination and water treatment—past, present and future (a review). *Desalination***2008**, *228*, 10–29.

(10) Antonietti, M.; Fechler, N.; Fellinger, T. P. Carbon Aerogels and Monoliths: Control of Porosity and Nanoarchitecture via Sol-Gel routes. *Chem. Mater.***2014**, *26*, 196–210.

(11) El-Deen; A. G., Barakat, N.A.M.; Khalil, K. A; Kim; H. Y. Hollow carbon nanofibers as an effective electrode for brackish water desalination using the capacitive deionization process, *NewJ.Chem*., **2014**, *38*, 198-205.

(12) Wen,X.; Zhang,D.; Shi, L.; Yan, T.; Wang, H.;Zhang, J., Three-dimensional hierarchical porous carbon with a bimodal pore arrangement for capacitive deionization, *J. Mater. Chem.*, **2012**, *22*, 23835- 23844.

(13) Lei, H.; Yan, T.; Wang, H.; Shi, L.; Zhang, J.; Zhang,D. Graphene-like carbon nanosheets prepared by a Fe-catalyzed glucose-blowing method for capacitive deionization, *J. Mater. Chem. A*, **2015**,*3*, 5934-5941.

(14) Kim, C.; Lee, J.; Kim, S.; YoonJ. TiO_2 sol–gel spray method for carbon electrode fabrication to enhance desalination efficiency of capacitive deionization, *Desalination***2014**, *342*, 70–74.

(15) Wang, H.;Shi, L.; Yan, T.; Zhang, J.; Zhong Q.; Zhang,D. Design of graphene-coated hollow mesoporous carbon spheres as high performance electrodes for capacitive deionization, *J. Mater. Chem. A*, **2014**,*2*, 4739-4750.

(16) Wen,X.; Zhang,D.; Yan, T.; Zhang, J.; Shi, L. Three-dimensional graphene-based hierarchically porous carbon composites prepared by a dual-template strategy for capacitive deionization, *J. Mater. Chem. A*, **2013**, *1*, 12334–12344.

(17) Zhang,D.; Wen,X.; Shi, L.Yan, T.; Zhang, J.; Enhanced capacitive deionization of graphene/mesoporous carbon composites, *Nanoscale*, **2012**, *4*, 5440–5446.

(18) Wang, H.;Zhang,D.; Yan, T.; Wen,X; Zhang, J.; Shi, L.; Zhong Q. Three-dimensional macroporous graphene architectures as high performance electrodes for capacitive deionization. *J. Mater. Chem. A*, **2013**, *1*, 11778–11789.

(19) Yuan, P.; Liu, D.; Tan, D.-Y.; Liu, K.-K.; Yu, H.-G.; Zhong, Y.-H.; Yuan, A.-H.; Yu, W.-B.; He, H.-P. Surface silylation of mesoporous/macroporous diatomite (diatomaceous earth) and its function in Cu(II) adsorption: The effects of heating pretreatment. *Mic. Mes. Mat.***2013**, *170*, 9–19.

(20) Yuan, W.; Yuan, P.; Liu, D.; Yu, W.; Deng, L.; Chen, F. Novel hierarchically porous nanocomposites of diatomite-based ceramic monoliths coated with silicalite-1 nanoparticles for benzene adsorption . *Mic. Mes. Mat.***2015**, *206*, 184-193.

(21) Macías, C.; Rasines, G.; García, T.; Rodríguez, C.; Lavela, P.; Tirado, J.L.; Ania, C.O.; On the use of diatomite as antishrinkage additive in the preparation of monolithic carbon aerogels, *Carbon***2016**, *98*, 280-284.

(22) Shi, K.; Ren, M.; Zhitomirsky, I. Activated Carbon-Coated Carbon Nanotubes for Energy Storage in Supercapacitors and Capacitive Water Purification, *ACS Sustainable Chem. Eng.***2014**, *2*, 1289−1298.

(23) Rasines, G.; Lavela, P.; Macías, C.; Zafra, M. C.; Tirado, J. L.; Parra, J. B.; Ania C O. N-doped monolithic carbon aerogel electrodes with optimized features for the electrosorption of ions. *Carbon***2015**, *83*, 262–274.

(24) Zafra, M.C.; Lavela, P.; Rasines, G.; Macías, C.; Tirado, J.L.; Ania, C.O. A novel method for metal oxide deposition on carbon aerogels with potential application in capacitive deionization of saline water, *Electrochimica Acta***2014**, *135*, 208–216.

(25) Rasines, G.; Macías, C.; Haro, M.; Jagiello, J.; Ania, C.O. Effects of CO_2 activation of carbon aerogels leading to ultrahigh micro-meso porosity *Mic. Mes. Mat.***2015**, *209*, 18–22.

(26) Jagiello, J.; Olivier, J. P. 2D-NLDFT Adsorption Models for Carbon Slit-Shaped Pores with Surface heterogeneity and geometrical corrugation. *Adsorption***2013**, *19*, 777–783.

(27) Moulder, J. F. Stickle, W. F.; Sobol, P. E.; Bomben, K. D. *Book of Standard spectra for identification and interpretation of XPS data, Physical Electronics.* Minnesota: Eden Prairie; 1995.

(28) Job, N.; Théry, A.; Pirard, R.; Marien, J.; Kocon, L.; Rouzaud, J.N.; Béguin, F.; Pirard, J. P. Carbon aerogels, cryogels and xerogels: Influence of the drying method on the textural properties of porous carbon materials. *Carbon***2005**, *43*, 2481–2494.

(29) Gu, X.; Yang, Y.; Hu, Y.; Hu, M.; Wang, C. Fabrication of Graphene-Based Xerogels for Removal of Heavy Metal Ions and Capacitive Deionization *ACS Sustainable Chem. Eng.***2015**, *3*, 1056–1065.

(30) Macías, C.; Haro, M.; Parra, J.B.; Rasines, G.; Ania, C.O. Carbon-black directed synthesis of mesoporous aerogels. *Carbon***2013**, *63*, 487–497.

(31) Rasines, G.; Lavela, P.; Macías, C.; Zafra, M.C.; Tirado, J.L.; Ania, C.O. Mesoporous carbon black-aerogel composites with optimized properties for the electro-assisted removal of sodium chloride from brackish water, *J. Electroanal. Chem.***2015**, *741*, 42–50.

(32) Thommes, M.; Kaneko, K.; Neimark, A.V.; Olivier, J.P.; Rodriguez-Reinoso, F.; Rouquerol, J.; Sing, K.S.W. Physisorption of gases, with special reference to the evaluation of surface area and pore size distribution (IUPAC Technical Report) *Pure Appl. Chem.***2015**, *87*, 1051–1069.

(33) Sousa, J. P. S.; Pereira, M. F. R.; Figueiredo J. L. NO oxidation over nitrogen doped carbon xerogels. *Appl. Catal. B Environ.***2012**, *125*, 398–408.

(34) Singru, N. R.; Gurnule W. B.; Khati, V.A.; Zade, A. B.; Dontulwar, J. R. Eco-friendly application of p-cresol–melamine–formaldehyde polymer resin as an ion-exchanger and its electrical and thermal study. *Desalination***2010**, *263*, 200–210.

(35) Li, S.-M.; Yang, S.-Y.; Wang, Y.-S.; Lien, C.-H.; Tien, H.-W.; Hsiao, S.-T.; Liao, W.-H.; Tsai,H.-P.; Chang,C.-L.; Ma, C.-C. M.; Hu C.-C. Controllable synthesis of nitrogen-doped graphene and its effect on the simultaneous electrochemical determination of ascorbic acid, dopamine, and uric acid. *Carbon***2013**, *59*, 418–429.

(36) Yu, J.; Guo, M.; Muhammad, F.; Wang, A.; Yu, G.; Ma, H. Zhu, G. Simple fabrication of an ordered nitrogen-doped mesoporous carbon with resorcinol-melamine-formaldehyde resin. *Mic. Mes. Mat.***2014**, *190*, 117–127.

(37) Seredych, M.; Hulicova-Jurcakova, D.; Lu, G. Q.; Bandosz, T. J. Surface functional groups of carbons and the effects of their chemical character, density and accessibility to ions on electrochemical performance. *Carbon***2008**, *46*, 1475–1478.

(38) Terzyk, A. P. The influence of activated carbon surface chemical composition on the adsorption of acetaminophen (paracetamol) in vitro Part II. TG, FTIR, and XPS analysis of carbons and the temperature dependence of adsorption kinetics at the neutral pH. *Colloids Surf. A* **2001**, *177*, 23–45.

(39) Long, D.; Zhang, J.; Yang, J.; Hu, Z.; Cheng, G.; Liu, X.; Zhang, R.; Zhan, Li.; Qiao, W.; Ling L. Chemical state of nitrogen in carbon aerogels, issued from phenol–melamine–formaldehyde gels. *Carbon***2008**, *46*, 1259–1262.

(40) Huang, Y.; Yang, F.; Xu, Z.; Shen, J. Nitrogen-containing mesoporous carbons prepared from melamine formaldehyde resins with $CaCl_2$ as a template. *J Colloid Interface Sci.***2011**, *363*, 193–198.

(41) Ma, T. Y.; Dai, S.; Jaroniec, M.; Qiao, S. Z. Graphitic carbon nitride nanosheet–carbon nanotube three- dimensional porous composites as high-performance oxygen evolutionelectrocatalysts. *Angew. Chem. Int. Ed.***2014**, *53*, 7281–7285.

(42) Di Castro, V.; Polzonetti, G. XPS study of MnO oxidation. *J. Electron. Spectrosc. Relat. Phenom.***1989**, *48*, 117–123.

(43) Shi, F.; Wang, F.; Dai, H.; Dai, J.; Deng, J.; Liu, Y.; Bai, G.; Ji, K.; Au, C. T. Rod-, flower-, and dumbbell-like MnO_2: Highly active catalysts for thecombustion of toluene. *Applied Catalysis A: General* **2012**, *433–434*, 206–213.

(44) Liu, E.; Shen, H.; Xiang, X.; Huang, Z.; Tian, Y.; Wu, Y.; Wu, Z.; Xie, H. A novel activated nitrogen-containing carbon anode material for lithium secondary batteries. *Materials Letters***2012**, *67*, 390–393.

(45) Lu, Y.; Zhang, F.; Zhang, T. K.; Leng, L.; Zhang, X.; Yang , Y. M.; Huang, Y.; Zhang, M.; Chen. Y. Synthesis and supercapacitor performance studies of N-doped graphene materials using o-phenylenediamine as the double-N precursor. *Carbon***2013**, *63*, 508-516.

(46) Jeong, H. M.; Lee, J. W.; Shin, W. H.; Choi, Y. J.; Shin, H. J.; Kang, J. K.; Choi, J. W. Nitrogen-doped graphene for high-performance ultracapacitors and the importance of nitrogen-doped sites at basal planes. *Nano Lett***2011**, *11*, 2472–2477.

(47) Rasines, G.; Lavela, P.; Macías, C.; Haro, M.; Ania, CO.; Tirado, J. L. Electrochemical response of carbon aerogel electrodes in saline water. *J. Electroanal. Chem.***2012**, *671*, 92–98.

(48) Barbieri, O.; Hahn, M.; Herzog, A.; Kotz, R. Capacitance limits of high surface area activated carbons for double layer capacitors. *Carbon***2005**, *43*, 1303–1310.

TABLE OF CONTENTS GRAPHIC AND SYNOPSIS

Mn containing N-doped monolithic carbon aerogels with enhanced macroporosity as electrodes for capacitive deionization

Carlos Macías[1], Gloria Rasines[1], Pedro Lavela[2], María C. Zafra[2], José L. Tirado[2], Conchi O. Ania[3].*

Hybrid N- and Mn-doped carbon aerogels with enhanced conductivity and macroporosity evidencing optimized performance as electrodes for capacitive deionization.

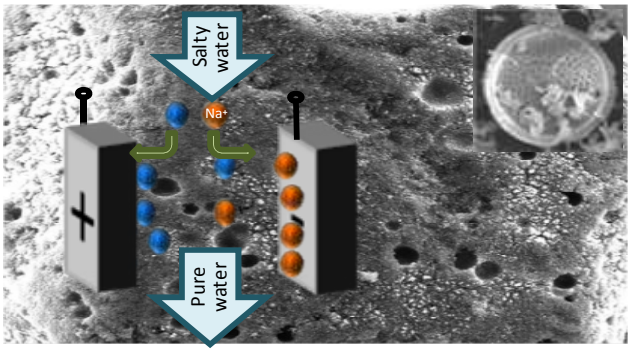

Supporting information

Mn containing N-doped monolithic carbon aerogels with enhanced macroporosity as electrodes for capacitive deionization

Gloria Rasines[1]*, Pedro Lavela[2]*, Carlos Macías[1], María C. Zafra[2], José L. Tirado[2], Conchi O. Ania[3]

[1] I+D Department, Nanoquimia S.L., PCT Rabanales 21, Ed. Aldebarán M.4.7. 14014 Córdoba, Spain

[2] Laboratorio de Química Inorgánica, Universidad de Córdoba, Marie Curie, Campus de Rabanales, 14071 Córdoba, Spain

[3]Adsorption and Environmental Remediation on Porous Solids (ADPOR), Instituto Nacional del Carbón, INCAR-CSIC, Apdo. 73, 33080 Oviedo, Spain.

Number of pages:**12**

Number of figures:**9**

Figure S1. Pictures of electrolyte droplets onto the carbon aerogel monoliths. The highly hydrophilic character of MRF-Mn-D and MRF-Mn-D-CB is revealed by a fast uptake preventing the picture capture of the electrolyte drop.

Figure S2. Transmission electron images of selected aerogels: a) MRF-Mn; b) MRF-Mn-D-CB.

Figure S3. X-ray diffraction pattern of MRF-Mn aerogel.

Figure S4. XPS spectra at C1s core levels of N-doped aerogels and their corresponding composites. a) MRF; b) MRF-Mn;c) MRF-Mn-D; d) MRF-Mn-D-CB.

Figure S5. XPS spectra at O1s core levels of N-doped aerogels and their corresponding composites. a) MRF; b) MRF-Mn;c) MRF-Mn-D; d) MRF-Mn-D-CB.

Figure S6. XPS spectra at N1s core levels of N-doped aerogels and their corresponding composites. a) MRF; b) MRF-Mn;c) MRF-Mn-D; d) MRF-Mn-D-CB.

Figure S7. Galvanostatic curves of MRF and MRF-Mn-D-CB a) charge and discharge profiles recorded at different current densities; b) discharge of MRF and MRF-Mn-D-CB at 0.1 A g^{-1}.

Figure S8**.** Comparison of the electrosorption capacity of the different carbon aerogels versus charge time and applied voltage.

Figure S9. Comparison of the electrosorption capacity for MRF,MRF-Mn-D and MRF-Mn-D-CBcarbon aerogels versus charge time. The values were recorded in cells chargedat 1.5 V in 0.1 M NaCl (ca.6 g/L) solution.

Number of tables: **1**

Table S1. Chemical composition (wt.%) determined by elemental analysis and XPS

spectroscopy of the synthesized carbon aerogels.

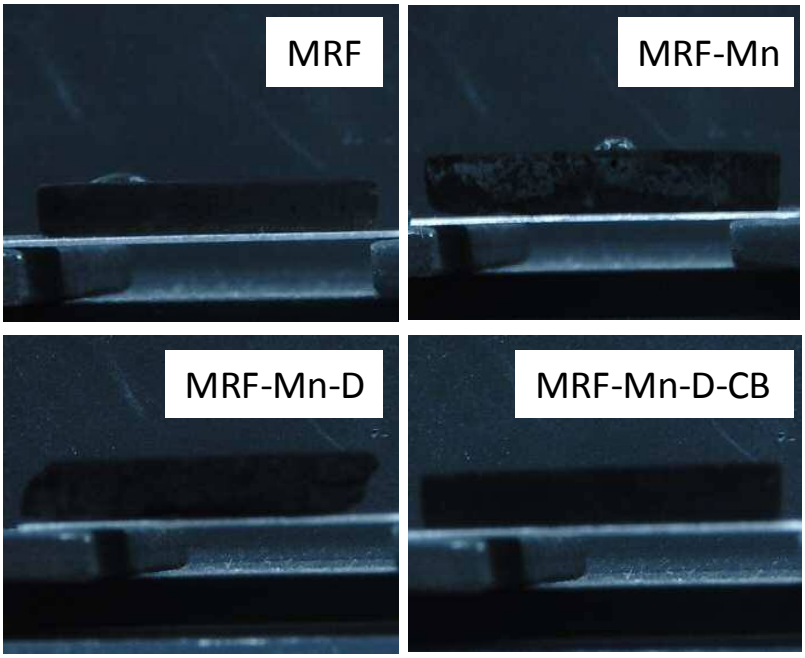

Figure S1. Pictures of electrolyte droplets onto the carbon aerogel monoliths. The highly hydrophilic character of MRF-Mn-D and MRF-Mn-D-CB is revealed by a fast uptake preventing the picture capture of the electrolyte drop.

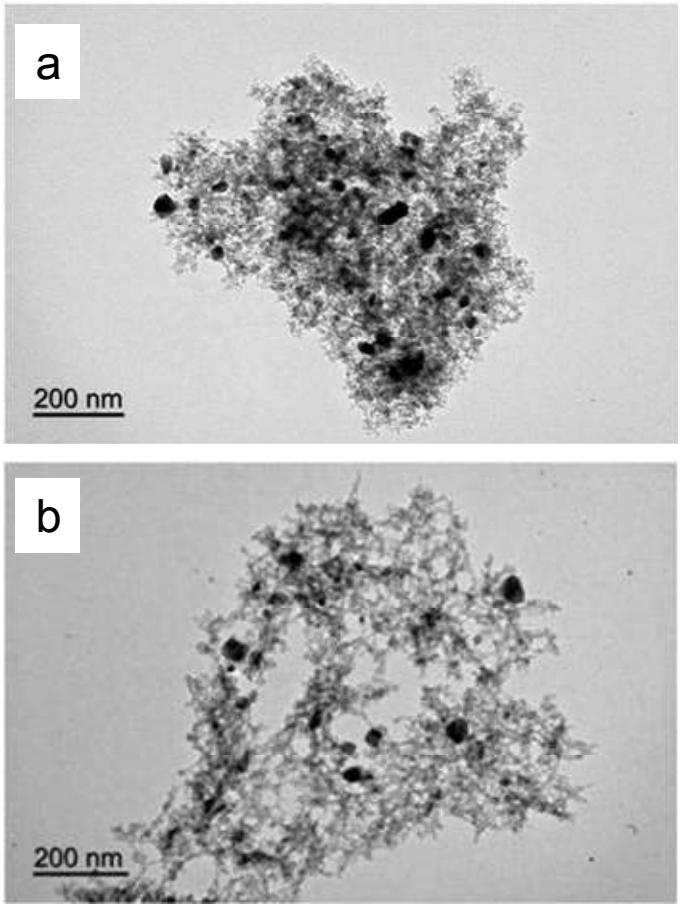

Figure S2. Transmission electron images of selected aerogels: a) MRF-Mn; b) MRF-Mn-D-CB.

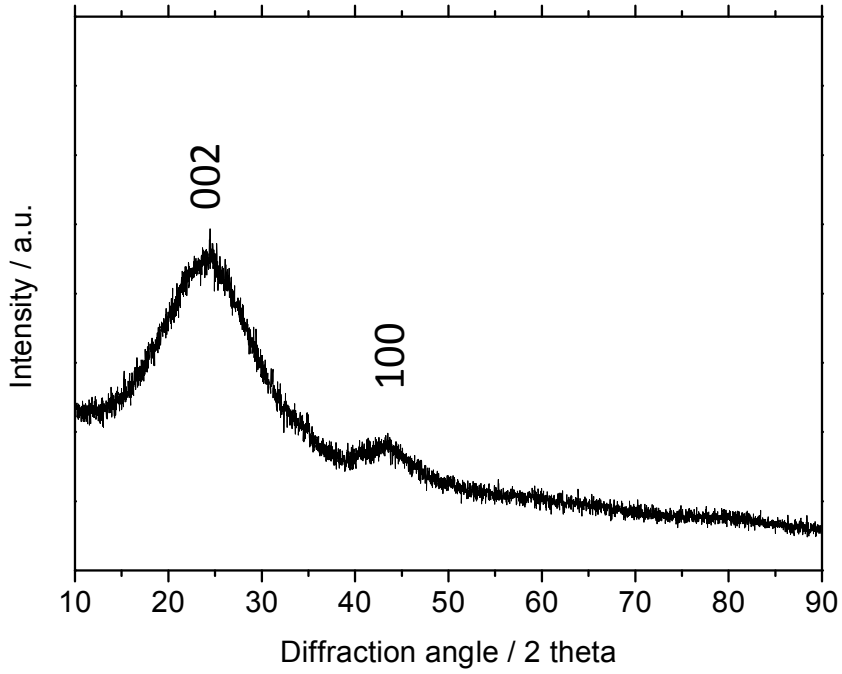

Figure S3. X-ray diffraction pattern of MRF-Mn aerogel.

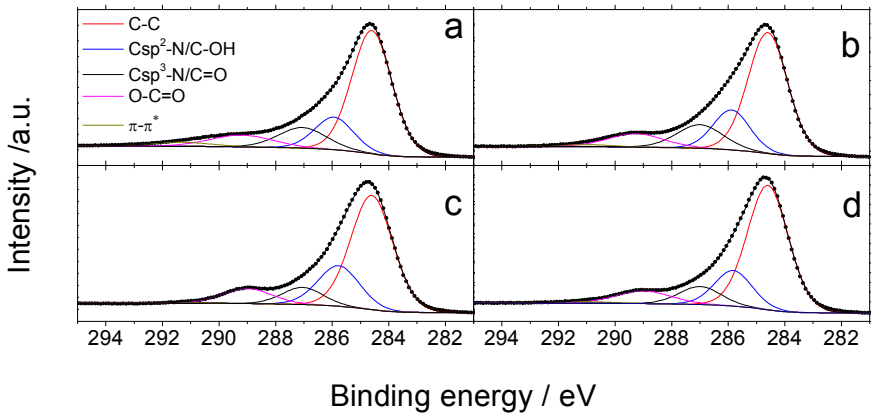

Figure S4. XPS spectra at C1s core levels of N-doped aerogels and their corresponding composites. a) MRF; b) MRF-Mn;c) MRF-Mn-D; d) MRF-Mn-D-CB.

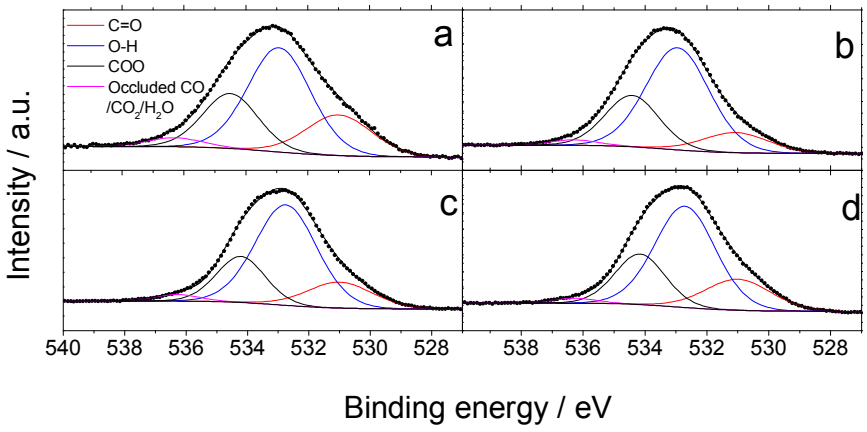

Figure S5. XPS spectra at O1s core levels of N-doped aerogels and their corresponding composites. a) MRF; b) MRF-Mn;c) MRF-Mn-D; d) MRF-Mn-D-CB.

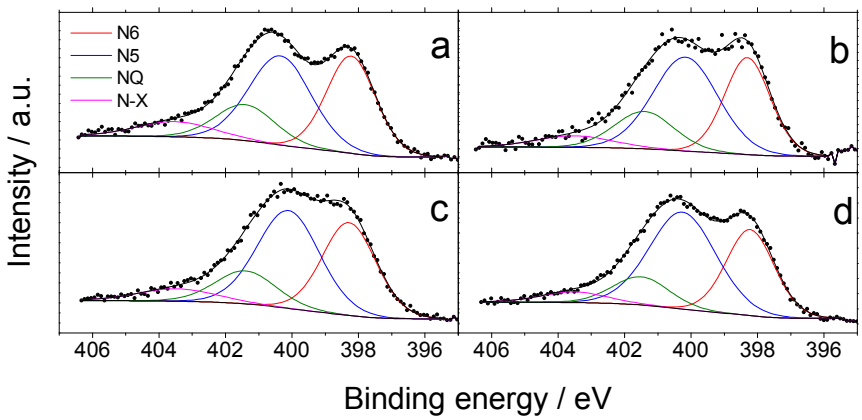

Figure S6. XPS spectra at N1s core levels of N-doped aerogels and their corresponding composites. a) MRF; b) MRF-Mn;c) MRF-Mn-D; d) MRF-Mn-D-CB.

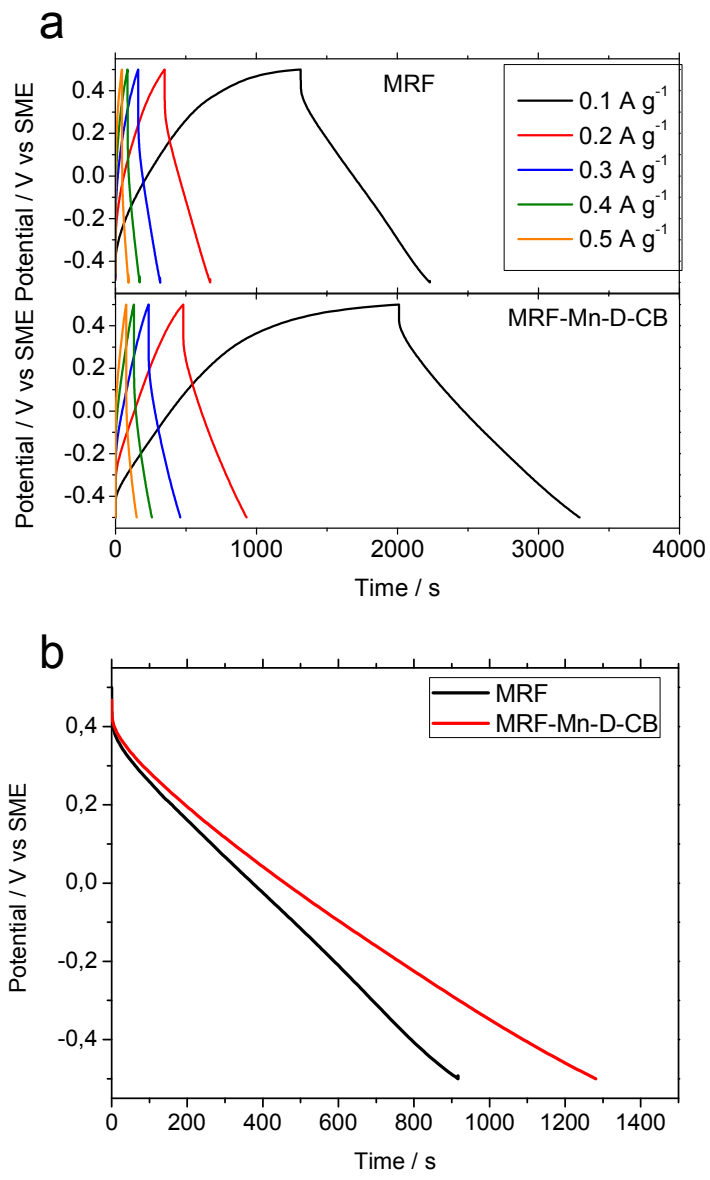

Figure S7. Galvanostatic curves of MRF and MRF-Mn-D-CB a) charge and discharge profiles recorded at different current densities; b) discharge of MRF and MRF-Mn-D-CB at 0.1 A g^{-1}.

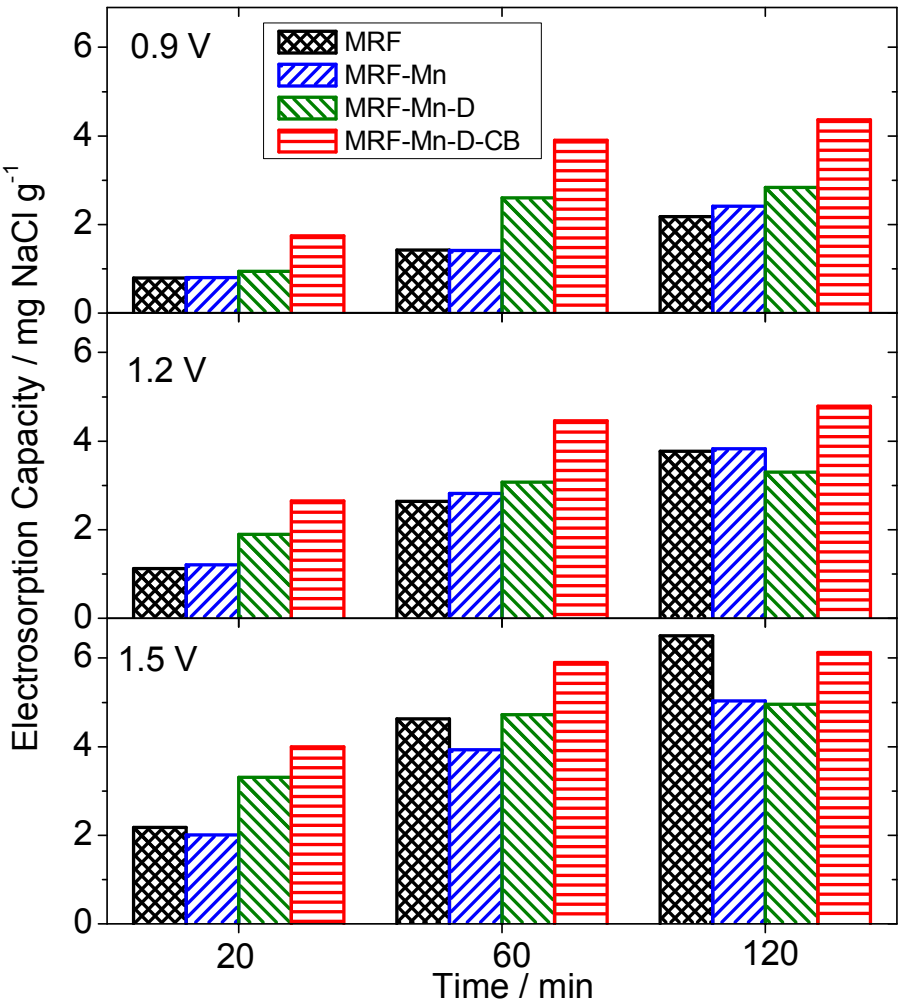

Figure S8**.** Comparison of the electrosorption capacity of the different carbon aerogels versus charge time and applied voltage.

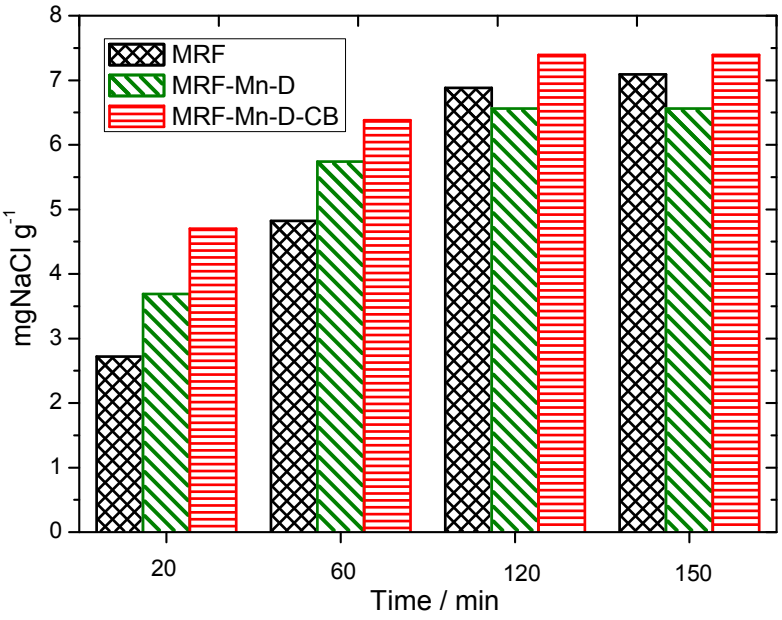

Figure S9. Comparison of the electrosorption capacity for MRF,MRF-Mn-D and MRF-Mn-D-CBcarbon aerogels versus charge time. The values were recorded in cells chargedat 1.5 V in 0.1 M NaCl (ca.6 g/L) solution.

Table S1. Chemical composition (wt.%) determined by elemental analysis and XPS spectroscopy of the synthesized carbon aerogels.

			XPS		
Sample	N/C ratio	N / %	C / %	O / %	Mn / %
MRF	0.04	3.2	87.5	9.3	
MRF-Mn	0.01	1.3	85.4	12.8	0.4
MRF-Mn-D	0.03	2.2	81.1	16.2	0.4
MRF-Mn-D-CB	0.03	2.3	84.8	12.4	0.5
			Elemental analysis		
Sample	N/C ratio	N / %	C / %		
MRF	0.06	4.5	79.9	--	--
MRF-Mn	0.05	3.6	73.9	--	--
MRF-Mn-D	0.06	3.5	61.6	--	--
MRF-Mn-D-CB	0.06	3.6	59.3	--	--